Rovibrational states calculations of the H₂O−HCN heterodimer with the Multiconfiguration Time Dependent Hartree method

Journal:	*Physical Chemistry Chemical Physics*
Manuscript ID	CP-ART-07-2023-003225.R3
Article Type:	Paper
Date Submitted by the Author:	27-Oct-2023
Complete List of Authors:	Tajouo Tela, Hervé; University of Rwanda, ICTP-East African Institute for Fundamental Research Quintas-Sánchez, Ernesto; Missouri University of Science and Technology, Chemistry Dubernet, Marie-Lise; Observatoire de Paris - Site de Meudon, LERMA scribano, yohann; Universite Montpellier Faculte des Sciences de Montpellier, LUPM Dawes, Richard; Missouri University of Science and Technology, Chemistry Gatti, Fabien; University Montpellier II, Institut Charles Gerhardt Ndengue, Steve; University of Rwanda, ICTP-East African Institute for Fundamental Research; Trinity College, Department of Physics

SCHOLARONE™
Manuscripts

PCCP

ARTICLE TYPE

Rovibrational states calculations of the H_2O–HCN heterodimer with the Multiconfiguration Time Dependent Hartree method

Hervé Tajouo Tela,[a] Ernesto Quintas-Sánchez,[b] Marie-Lise Dubernet,[c] Yohann Scribano,[d] Richard Dawes,[b] Fabien Gatti,[e] and Steve Ndengué[a‡]

Water and hydrogen cyanide are two of the most common species in space and the atmosphere with the ability of binding to form dimers such as H_2O–HCN. In the literature, while calculations characterizing various properties of the H_2O–HCN cluster (equilibrium distance, vibrational frequencies and rotational constants) have been done in the past, extensive calculations of the rovibrational states of this system using a reliable quantum dynamical approach have yet to be reported. In this work, we intend to mend that by performing the first calculation of the rovibrational states of the H_2O–HCN van der Waals complex on a recently developed potential energy surface. We use the Block Improved Relaxation procedure implemented in the Heidelberg MultiConfiguration Time-Dependent Hartree (MCTDH) package to compute the states of the H_2O–HCN isomer, from which we extract the transition frequencies and rotational constants of the complex. We further adapt an approach first suggested by Wang and Carrington—and supported here by analysis routines of the Heidelberg MCTDH package—to properly characterize the computed rovibrational states. The subsequent assignment of rovibrational states was done by theoretical analysis and visual inspection of the wavefunctions. Our simulations provide a Zero Point Energy (ZPE) and intermolecular vibrational frequencies in good agreement with past *ab initio* calculations. The transition frequencies and rotational constants obtained from our simulations match well with the available experimental data. This work has the broad aim to propose the MCTDH approach as a reliable option to compute and characterize rovibrational states of van der Waals complexes such as the current one.

1 Introduction

Water (H_2O) and hydrogen cyanide (HCN) are common components of planetary and interstellar environments,[1–3] contributing significantly to their rich chemistry. For instance, H_2O is the most abundant molecule in cometary atmospheres and HCN is amongst the few dozen molecules that have been observed around comets. Furthermore, hydrogen bonding is a fundamental phenomenon in chemistry, and its importance has been widely recognized in

various fields of study, including atmospheric chemistry, biological processes, catalytic reactions, and materials science.[4–7] The HCN molecule is scientifically fascinating for multiple reasons. It is a highly anharmonic system that possesses a wide range of vibrational states, which combined with its triatomic nature, makes it a convenient model-system for the accurate study of predissociation and to develop/test theoretical methodologies that can be applied to more complex systems.[8,9] The H_2O−HCN is a relevant complex in astrophysics,[9,10] composed of two common molecules in planetary environments and comets.[1,2] In the Interstellar Medium (ISM) system, H_2O is also one of the most abundant molecules after CO and H_2.

The interaction between water and hydrogen cyanide has been extensively studied,[11–16] with a special interest in the theoretical investigation of its structure and spectroscopy. This interaction leads to two different isomers. In one, HCN acts as the proton donor ($H_2O\cdots HCN$), and in the other one HCN acts as the proton acceptor ($HCN\cdots H_2O$), as shown in Figure 1, with the $H_2O\cdots HCN$ isomer being the more stable.[17–19] Moreover,

[a] *ICTP-East African Institute for Fundamental Research, University of Rwanda, Kigali, Rwanda.*

[b] *Department of Chemistry, Missouri University of Science and Technology, 65409 Rolla, Missouri, United States.*

[c] *LERMA, Observatoire de Paris, PSL Research University, CNRS, Sorbonne University, UPMC Univ Paris 06, 75014 Paris , France.*

[d] *Laboratoire Univers et Particules de Montpellier, UMR-CNRS 5299, Université de Montpellier, Place Eugène Bataillon, 34095 Montpellier, France.*

[e] *Institut de Sciences Moléculaires d'Orsay, UMR 8214, Université Paris-Sud - Université Paris-Saclay, 91405 Orsay, France.*
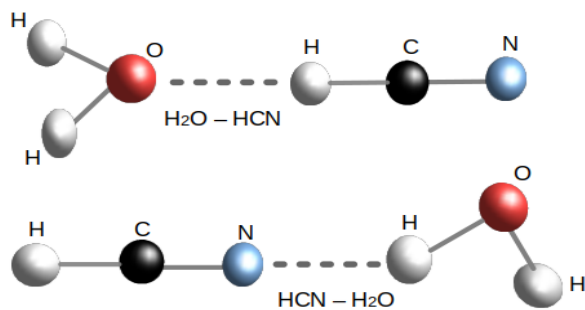
‡ Email:sndengue@eaifr.org

Fig. 1 Structures of H_2O−HCN (corresponding to the global minimum) and HCN−H_2O (corresponding to the secondary minimum) isomers.

the isomerization reaction between water and hydrogen cyanide has been studied (using high-level *ab initio* calculations[20,21] and microwave spectroscopy[22,23]) as well as for its isotopes[11] (using the pulsed-nuzzle technique, Fourier-transform microwave spectroscopy and a modified Balle/Flygare Fourier-transform microwave spectrometer associated with a sample source pulsed supersonic nozzle).

While numerous works in the past two decades have surveyed (some even in full dimensionality) the rovibrational states of water containing heterodimers with linear molecules of astrophysical relevance (such as H_2O–H_2,[24–26] H_2O–CO,[27–32] H_2O–HF,[33–35] H_2O–CO_2[36] and H_2O-HCl,[37–39] just to name a few) there is to our knowledge no published report of rovibrational states calculations for the H_2O−HCN system, either in full dimensionality nor even in the rigid rotor approximation. Not even after the publication of a new state-of-the-art five-dimensional potential energy surface (PES) of H_2O−HCN by Quintas-Sánchez and Dubernet[15] (referred to as the QSD PES later in the text); which, despite being built primarily for astrophysical simulations, turn out—as we will show here—to be quite reliable for spectroscopic studies as well.

We present in this work the first calculations of the low-lying rovibrational states for the H_2O−HCN complex, obtained using the MultiConfiguration Time-Dependent Hartree (MCTDH) method. The paper is organized as follows. In the next section, we describe the methodology and computational procedure followed for the MCTDH calculations. Following that, in another section, we present and discuss our results. Finally, we summarize our work and discuss future avenues of research for this system and others.

2 Computational procedure

2.1 Rovibrational states calculations with MCTDH

The rovibrational spectrum of the H_2O–HCN cluster is studied using the MCTDH algorithm.[40–43] MCTDH is a time-dependent method in which each degree of freedom is associated with a small number of orbitals (or single-particle functions, SPFs) which, through their time dependence, allow an efficient description of the molecular dynamical processes. The total MCTDH wave function is expanded in Hartree products, that is, products

of SPFs:

$$\Psi(Q_1,\ldots,Q_f,t) = \sum_{j_1=1}^{n_1} \cdots \sum_{j_f=1}^{n_f} A_{j_1\cdots j_f}(t) \prod_{\kappa=1}^{f} \phi_{j_\kappa}^{(\kappa)}(Q_\kappa,t)$$

$$= \sum_\Lambda A_\Lambda \Phi_\Lambda \,, \tag{1}$$

where f is the number of degrees of freedom (DOF) of the system, $Q_1,\ldots,Q_f$ are the nuclear coordinates, $A_\Lambda \equiv A_{j_1\cdots j_f}$ denotes the MCTDH expansion coefficients, and $\phi_{j_\kappa}^{(\kappa)}(Q_\kappa,t)$ are the n_κ SPFs associated with each degree of freedom κ (*i.e.*, they form a time dependent variable basis along κ). The subsequent equations of motion for the coefficients and SPFs are derived after substituting the wave function *ansatz* into the time-dependent Schrödinger equation. To solve the equations of motion, the κ SPFs are represented on a (fixed) primitive basis or discrete variable representation (DVR)-grid[44–46] of N_κ points:

$$\varphi_{j_\kappa}^{(\kappa)}(Q_\kappa,t) = \sum_{i_\kappa=1}^{N_\kappa} c_{i_\kappa j_\kappa}^{(\kappa)}(t)\chi_{i_\kappa}^{(\kappa)}(Q_\kappa) \,, \tag{2}$$

where ideally the n_κ of eqn 1 is such that $n_\kappa << N_\kappa$. Thus, the MCTDH method propagates the wave function on a small, time-dependent, variationally optimized basis set of single-particle functions, which in turn are defined on a fixed time-independent primitive basis set.

The MCTDH algorithm is more efficient when the Hamiltonian operator is written as a sum of products (SOP) of single-particle operators. The Kinetic Energy Operator (KEO) can easily be expressed in the required form when using polyspherical coordinates, such as the Jacobi coordinates used in this work. We followed the subsystem KEO derivation presented by Gatti and Iung,[47] which was used in some of our previous work to describe an asymmetric rotor–atom collision[48] and an asymmetric rotor–diatom collision and spectroscopy.[26,49] In the specific case of dimers, this separation of subsystem is similar to the formulation for dimers given in the seminal work by Brocks *et al.*[50] As we did in our previous MCTDH calculations,[51] we do not work in the Body-Fixed (BF) frame but in the E_2 frame,[26,47] which is obtained by rotation of the two first Euler angles of the SF frame (*cf.* figures 2 and 3). This representation leads to a decoupling of the modes of each monomer and is particularly useful for inelastic calculations with the MCTDH approach.[49] The KEO in the E_2 frame can be expressed as

$$2\hat{T} = -\frac{1}{\mu_R}\frac{\partial^2}{\partial R^2} + 2\hat{T}_A + 2\hat{T}_B$$

$$+ \frac{1}{\mu R^2}\left(\vec{J}^\dagger\vec{J} + (\vec{L}_A+\vec{L}_B)^2 - 2(\vec{L}_A+\vec{L}_B)\vec{J}\right)_{E_2}, \tag{3}$$

where μ_R is the reduced mass of the H_2O–HCN cluster, and the A and B subscripts refer to the H_2O and HCN fragments respectively. The rigid rotor Hamiltonian of the H_2O molecule is expressed

as [52,53]

$$\hat{T}_A = \frac{A}{2}\left(L_{A,+}^2 + L_{A,-}^2 + L_{A,+}L_{A,-} + L_{A,-}L_{A,+}\right)$$

$$-\frac{C}{2}\left(L_{A,+}^2 + L_{A,-}^2 - L_{A,+}L_{A,-} - L_{A,-}L_{A,+}\right)$$

$$+BL_{z_{BF_A}}^2, \tag{4}$$

with the H_2O rotational constants: $A = 27.88063$ cm^{-1}, $B = 9.27771$ cm^{-1} and $C = 14.52177$ cm^{-1}.[54] The rigid rotor kinetic energy of the HCN fragment can be written simply as $\hat{T}_B = B_{HCN}\vec{L}_B^2$, with the rotational constant $B_{HCN} = 1.4782218$ cm^{-1}.[55,56] The reduced mass used for the H_2O-HCN system was $\mu = 10.805547045$ a.m.u.

The final form of the KEO as implemented in the MCTDH code is then

$$2\hat{T} = -\frac{1}{\mu_R}\frac{\partial^2}{\partial R^2} + 2\hat{T}_A + 2\hat{T}_B$$

$$+\frac{1}{\mu R^2}\left(J(J+1) + \vec{L}_A^2 + \vec{L}_B^2 - 2L_{A,z}^2 - 2L_{B,z}^2\right)$$

$$+\frac{1}{\mu R^2}\left(L_{A,+}L_{B,-} + L_{A,-}L_{B,+} - 2L_{A,z}L_{B,z}\right)$$

$$+\frac{1}{\mu R^2}\left(C_+(J,K)(L_{A,+} + L_{B,+})\right)$$

$$+\frac{1}{\mu R^2}\left(C_-(J,K)(L_{A,-} + L_{B,-})\right), \tag{5}$$

with

$$C_{\pm}(J,K) = \sqrt{J(J+1) - K(K\pm1)}. \tag{6}$$

2.2 The Potential Energy Surface

The potential energy operator, just as the KEO, also needs to be expressed in a sums of products form. Usually, for systems of the appropriate dimension (< 6) for which the PES is not expressed in the product-form already, there exists an efficient fitting procedure (Potfit,[57,58] implemented in the MCTDH package[59]) to obtain the appropriate representation. For potentials in even higher dimensionality, a MultiGrid Potfit,[60] a Multi-Layer Potfit,[61] or even more recently, a Monte-Carlo implementation of the Canonical Polyadic Decomposition (CPD)[62] for MCTDH are now available to transform general potentials into a product form. However, some of these implementations can lead to a prohibitive number of terms in the potential expansion—and thus slow down computations—while for others the handling of the system's symmetries becomes problematic—and thus may restrict, or poorly represent, the whole range of the potential for this type of application. In this study, just as we did in our previous work for H_2O-H$_2$,[26] we overcome this problem by taking advantage of the fact that the potential is already represented in a multipolar form[15] and that we only have to make a transformation to re-express it in coordinates more suitable for the MCTDH calculations.
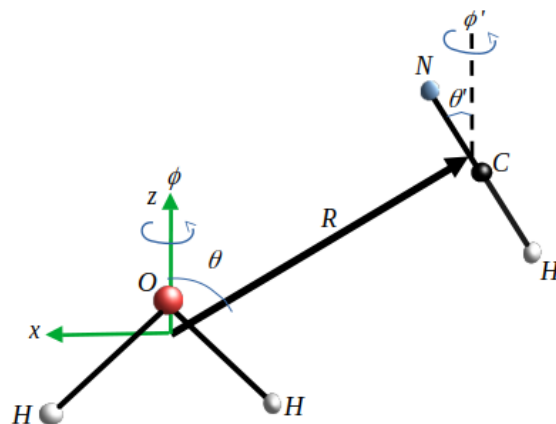

Fig. 2 Definition of the dimer BF coordinates system used in Ref. 15 to represent the PES of the H_2O-HCN system.

The PES from Ref. 15 is originally expressed as:

$$V(R,\theta,\varphi,\theta',\varphi') = \sum_i v_i(R)\bar{t}_i(\theta,\varphi,\theta',\varphi'), \tag{7}$$

with $i = \{l_A, m_A, l_B, l\}$, and

$$\bar{t}_i(\theta,\varphi,\theta',\varphi') = \frac{1}{2\pi}\alpha_{l_A,m_A}\sum_{r_1=-l_A}^{l_A}\sum_{r_2=-l_B}^{l_B}\beta_{i,r_1}\begin{pmatrix} l_A & l_B & l \\ r_1 & r_2 & r \end{pmatrix}$$

$$\times P_{l_B}^{r_2}(cos\theta')P_l^r(cos\theta)cos(r_2\varphi' + r\varphi), \tag{8}$$

where the expression in large brackets is a Wigner 3-j symbol, and the factors α_{l_A,m_A} and β_{i,r_1} are given by:

$$\alpha_{l_A,m_A} = \frac{\sqrt{2l_A+1}}{\sqrt{2+2\delta_{m_A,0}}}, \tag{9}$$

and

$$\beta_{i,r_1} = \frac{1}{2\pi}\left(\delta_{m_A,r_1} + (-1)^{l_A+m_A+l_B+l}\delta_{-m_A,r_1}\right). \tag{10}$$

Indices r_1, r_2, and r are dependent through $r = -(r_1+r_2)$. The maximum order of the terms involved in the expansion are determined by $l_A = 7$, $l_B = 12$, $m_A = 4$, and $l = 18$ (with $m_A \geq 0$, and l_A and $l_A + l_B + l$ always being even because of symmetry considerations) resulting in a total of 445 one-dimensional $v_i(R)$ terms in eqn 7. The angles (θ,φ) and (θ',φ') represent respectively the collisional direction and the HCN fragment orientation in the BF frame, as represented in Figure 2. As can be seen in the figure, the BF of the original PES is defined such that its origin is the center of mass of the H_2O molecule, the z-axis is its C_2 axis, with the positive z in the direction of the O atom and the xz plane being the plane containing the H_2O molecule.

Figure 4 shows a two-dimensional cut of the QSD PES as a function of R and θ (the other three angular coordinates are fixed at their corresponding values for the global minimum: $\varphi = 0°$, $\theta' = 0°$, and $\varphi' = 0°$). Notice that the global minimum of the potential—corresponding to the $H_2O\cdots$HCN isomer— is located at the bottom of the figure ($\theta = 0°$ and $R = 7.162$ Å), with a well depth of 1814.51 cm^{-1}. A secondary minimum (not shown in
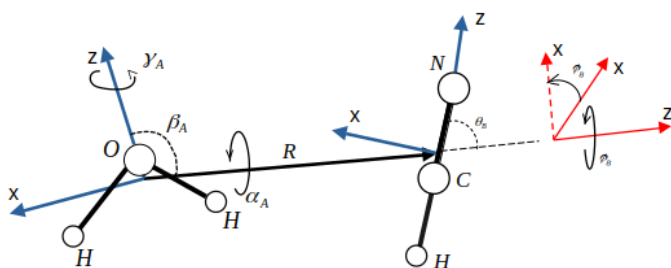
Fig. 3 Definition of the H_2O-HCN in the rigid rotor approximation and coordinates system used to compute the rovibrational states.
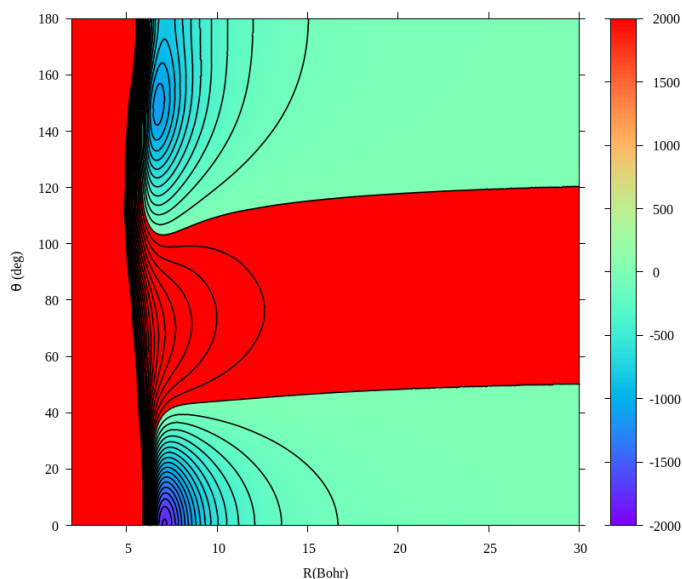

Fig. 4 2D cut of the PES. The figure shows the global (De=1814.51 cm^{-1} for H_2O-HCN isomer)

the figure) corresponding to the $HCN \cdots H_2O$ isomer, is located at $\theta = 119.61°$, $\varphi = 0°$, $\theta' = 74.49°$, $\varphi' = 180°$ and $R = 7.004$ Å, with a well depth of 1377.30 cm^{-1}.

In the MCTDH implementation, the dynamics of this system in the E_2 frame is described by six coordinates: the fragments' separation R and five angles (α_A, β_A, γ_A, θ_B and φ_B), as shown in Figure 3. The origin of the E_2 frame is the center of mass of H_2O, as it was the case for the BF frame. The z-axis is in the direction of $\vec{R}$, the vector connecting the centers of mass of the two molecules (cf. Figure 3). The three Euler angles (α_A, β_A, γ_A) determine the orientation of the H_2O molecule in our E_2 frame, while the other two spherical angles (θ_B and φ_B) define the orientation of the HCN molecule.

As van der Avoird and Nesbitt pointed out,[24] there are two ways to transform the PES coordinates from the BF Frame to the E_2 Frame. In the first approach, the coordinates are related according to $\theta = \beta_A$; $\phi = \pi - \gamma_A$; and θ', ϕ' can be expressed in terms of $\alpha_A, \beta_A, \gamma_A, \theta_B, \phi_B$ with the use of an inverse Euler rotation matrix;[24] then, the PES in the appropriate frame can be numerically

generated. This procedure, used by Wang and Carrington,[25] is not convenient for this work as it would require building a new SOP expansion of the PES after the surface is numerically transformed. We should point out that our BF and E_2 Frames correspond respectively to the Molecule Fixed (MF) and the Dimer Fixed (DF) Frames described in the work of Wang and Carrington. The second approach, which is the one we used, relates the coefficients of the multipolar expansion in both frames[24] and thus allows to generate the PES in the E_2 Frame directly in a SOP form. The correctness of the new multipolar expansion in the E_2 Frame can be conveniently verified by comparing the new PES values with the corresponding ones generated using the original PES. This approach saves a significant amount of time and allows more flexibility in the calculations. It is worth noticing that this transformation was already tested and checked in our previous work on $H_2O–H_2$,[26] which used a multipolar PES constructed with the same type of coordinates as the ones used by Quintas-Sánchez and Dubernet.[15]

2.3 Details of the computations

The rovibrational bound states of the $H_2O–HCN$ complex are obtained with the block improved relaxation method[42,63] implemented in the Heidelberg MCTDH package.[59] The block improved relaxation is derived from the improved relaxation method,[64,65] a MCSCF approach where the SPFs are optimized by relaxation[66] (propagation in negative imaginary time) but the coefficients vector (A-vector) is determined by diagonalization of the Hamiltonian matrix evaluated in the set of present SPFs using the Davidson algorithm.[67] MCTDH is, thus, used here as a time-independent method, where however the optimized basis functions are obtained by relaxation, a time dependent approach. The working equations of the improved relaxation and block improved relaxation have already been extensively described elsewhere[42,64,65] and do not need to be repeated here.

The primitive basis, its range, and the number of SPFs used for the calculations of the rovibrational states are summarized in Table 1. We performed all the calculations reported in this work using the block improved relaxation method—proceeding in blocks of three states, starting from the ground state and progressing to highly excited states. The relaxation time for a converged calculation with a block of three wavefunctions took approximately 72 hours of computational time using 16 processors on a Linux Cluster. For the evaluation of levels with $J > 0$, one could start the calculations from the previously converged results corresponding to $J - 1$, and thus save a significant amount of computational time to reach convergence. To describe the orientation of the H_2O and the HCN fragments in the E_2 frame, a primitive basis composed of Fast Fourier Transform (FFT) functions for the intermolecular distance R, was coupled with a Wigner-DVR basis for β_A, and a two-dimensional extended Legendre-K DVR (replacing ϕ_B by k_ϕ), while α_A and γ_A are replaced by their momentum representation k_α and k_γ. For testing purposes, we also ran ($J = 0$) calculations with the angular primitive basis composed of the Wigner-DVR basis and a two-dimensional Legendre DVR. The (Wigner, K, K) and (KLeg, K) DVRs are thus replaced in these tests by their counter-

parts the (Wigner, Exp, Exp) and (PLeg, Exp) DVRs, where KLeg and PLeg are respectively the extended Legendre DVR and two dimensional Legendre DVR. As mentioned in our previous work,[26] while calculations in real space coordinates basis at $J = 0$ may be slightly faster than calculations in real and momentum basis, we used the real and momentum basis because it is the only one that allows $J > 0$ calculations with the MCTDH description of our chosen frame and operators.

After transforming the PES from eqn (7) to the E_2 frame, we can write

$$V(R, \beta_A, \gamma_A, \alpha_A, \theta_B, \phi_B) = \sum_{\substack{r_\beta, r_\gamma \\ r_\alpha, r_\theta \\ r_\alpha, r_\theta}} \bar{V}_{\substack{r_\beta, r_\gamma \\ r_\alpha, r_\theta}}(R) f_{\substack{r_\beta, r_\gamma \\ r_\alpha, r_\theta}}(\omega_A, \omega_B) \qquad (11)$$

where

$$f_{\substack{r_\beta, r_\gamma \\ r_\alpha, r_\theta}}(\omega_A, \omega_B) = D_{r_\alpha r_\gamma}^{(r_\beta)}(\alpha_A, \beta_A, \gamma_A)^\star C_{r_\theta, -r_\alpha}(\theta_B, \phi_B) \qquad (12)$$

with $D_{r_\alpha r_\gamma}^{(r_\beta)}(\alpha_A, \beta_A, \gamma_A)$ and $C_{r_\theta, -r_\alpha}(\theta_B, \phi_B)$ being respectively the Wigner D-matrix and the Racah normalized spherical harmonics. The action of the potential on the wavefunction can then be obtained using k_α, k_γ and k_ϕ to express the angles α_A, γ_A, and ϕ_B. In the following, we drop the indices A and B for simplicity.

$$\hat{V}\Psi(R, \beta, k_\gamma, k_\alpha, \theta, k_\phi) = \sum_{\substack{r_\beta, r_\gamma \\ r_\alpha, r_\theta}} \bar{V}_{\substack{r_\beta, r_\gamma \\ r_\alpha, r_\theta}}(R, \beta, k_\gamma, k_\alpha, \theta, k_\phi) \qquad (13)$$

$$\times \Psi(R, \beta, k_\gamma - r_\gamma, k_\alpha - r_\alpha, \theta, k_\phi + r_\alpha).$$

We selected the primitive basis set by testing the convergence of the low-lying energy levels for various choices of the DOF parameters. The ones reported in Table 1 yield convergence of the results to within 0.02 cm^{-1} or less for the low-lying states. Also, the number of SPFs was increased in the calculations from a relatively small number for the lower levels to significantly larger values for the excited states: this grows quickly because of the deep well of the potential and the rapidly growing density of states with increasing energy.

A point of emphasis to ease the reading of this manuscript: in the following sections, J, K will relate to the rotation of the dimer, while j, k will be associated to the rotation of the H$_2$O monomer.

The Wigner-DVR can be implemented in two forms in MCTDH. In one, the 3 Euler angles can be used as they are defined to characterize each of the degrees of Freedom of the Wigner-DVR. In the other, the α and γ angles could be Fourier Transformed into the K component used in the calculations. This approach is also used with the Extended Legendre DVR implemented in MCTDH where the azimuthal angle can be Fourier Transformed and limited to values smaller than the expected size of the primitive basis: we did it also for this work.

2.4 Symmetry and assignment of states

The current implementation of the Wigner-DVR in the MCTDH package does not allow even/odd symmetry differentiation while performing the calculations using a direct product basis. Hence, it was not possible to selectively compute (ro)vibrational states that have a specific symmetry with respect to the H$_2$O fragment

axis. Nevertheless, using the computational procedure described above we are able to obtain a large number of states (some real and some fictitious) which can be challenging to assign directly. In previous calculations of this type of cluster, such as the H$_2$O−H$_2$ calculations performed by van der Avoird and Nesbitt,[24] or Wang and Carrington,[25] the primitive basis was constrained such that K, the projection of the total angular momentum, satisfies: $K = m_A + m_B$. Wang and Carrington proposed a method to characterize the rovibrational states according to the abundance of the character of the rigid rotor rotational state of H$_2$O in the wavefunction: that is, characterizing it along the most abundant $j_{k_a k_c}$, where k_a and k_c are the projections of the total angular momentum J on the inertial axis in the prolate and oblate limits.

In this work, we are able to go beyond the analysis we performed previously on a similar system[26] (H$_2$O–H$_2$) to do a characterization in a similar fashion as Wang and Carrington.[25] First, as we did in our previous work on H$_2$O–H$_2$, the Σ, Π, ... characters of the wavefunction can be extracted after the MCTDH calculation by looking at the output file of a single state calculation. Here, by summing the average values of the α and ϕ DOFs (which correspond to the m_A and m_B used by Wang and Carrington), we can determine K as $K = \langle \alpha \rangle + \langle \phi \rangle$. This approach not only makes it possible to determine K but also turns out to filter physical states from fictitious ones; since we are using a direct basis with no constraints on the basis functions, the computational procedure is free to generate for instance for $J = 0$, states having a projection $K > 0$ which is not physical. By applying the $K = \langle \alpha \rangle + \langle \phi \rangle$ criterion, we can discard all the nonphysical states from the results. In Table 3, we show the lowest 8 states from a block improved relaxation calculation, where 6 of the 8 are nonphysical.

The H$_2$O character ($j_{k_a k_c}$) of the rovibrational state was obtained by projection of the rovibrational wavefunction onto the rotational states of H$_2$O. The specific $j_{k_a k_c}$ character presented in Tables 4–7 was assigned by selecting the largest projection of the rovibrational state to the H$_2$O rotational states considered. The projection of the rovibrational state $|\Psi\rangle$ is obtained from the relation $p_i = \langle \Psi | \hat{P}_i | \Psi \rangle$, where the projector $\hat{P}_i$ onto a rovibrational state $|j_{k_a k_c}, m\rangle$ writes $\hat{P}_i = |j_{k_a k_c}, m\rangle \langle j_{k_a k_c}, m|$. The contributions of each projection $|j_{k_a k_c}, m\rangle$ are then summed to obtain the contribu-

Table 1 Parameters of the primitive basis used for the rovibrational calculations of H$_2$O−HCN. FFT stands for the Fast Fourier Transform. Wigner stands for the Wigner DVR. KLeg is the extended Legendre DVR. K stands for the momentum representation of a set of angles: the first and third Euler angles α_A and γ_A of H$_2$O, and the second spherical angle ϕ_B of HCN, both monomers in the rigid rotor approximation. The units for distance and angle are Bohrs and radians respectively. We additionally would like to stress that the range of γ_A, α_A and ϕ_B are actually the ranges of their respective momentum representation k_γ, k_α and k_ϕ respectively.

Coordinate	Primitive Basis	Number of Points	Range	Size of SPF basis
R	FFT	96	2.0–22.0	10–20
β_A	Wigner	12	0–π	20–100
γ_A	K	23	-11,11	
α_A	K	11	-5,5	
θ_B	KLeg	24	0–π	40–60
ϕ_B	K	11	-5,5	

tion of the $|j_{k_a k_c}\rangle$ rotational state to the wavefunction. Additional details on this derivation are provided in the Appendix.

3   Results and Discussion

The primary motivation of this work is the lack of availability in the literature of work reporting calculations of rovibrational states of the H_2O-HCN complex with only a couple of exceptions. We also independently performed here ab initio calculations at a higher level of theory (CCSD(T)-F12) to serve as a basis of comparison for the rovibrational state ($J = 0$) calculations.

3.1   Comparison with harmonic frequencies

A limited number of published results on the vibrational states of H_2O-HCN are available in the literature. So far, only harmonic frequencies[14,68] have been reported for this system and some of its isotopologues/isotopomers. This limits the validation of our new results. Nevertheless, in Table 2 we compare the previously reported harmonic frequencies obtained by Heikkilä et al.[14] (2nd order Møller–Plesset perturbation theory (MP2) with 6-311++G(2d,2p)) and Tshehla and Anthony[68] (MP2 with 6-31G** split-valence polarized basis set) with our new CCSD(T)-F12b/VTZ-F12 harmonic frequencies and the full variational vibrational frequencies ($J = 0$) obtained from MCTDH using the QSD PES.

The four different approaches compared in the table exhibit significant, but not drastic, variations between each of the three sets of harmonic frequencies as well as with the full MCTDH calculations. Of course harmonic frequencies are notoriously inaccurate for low frequency modes corresponding to large amplitude motion. This particular complex is somewhat more tightly bound with its rather large well depth, so the comparison is still sensible. Of the three harmonic calculations, the CCSD(T)-F12 method employed in our new calculations is most similar to that underlying the QSD PES, yet especially for certain modes there are significant differences between those harmonic frequencies and the more complete MCTDH results.

The MCTDH rovibrational calculations reflect the quality of the electronic structure calculations (CCSD(T) with counterpoise correction for basis set superposition error) and fitting quality of the QSD PES. The significant variation observed, most notably for the HCN libration and H_2O torsion modes, is not surprising given the different methods employed, but points to the valuable contribution that an experimental measurement could make.

The assignment of the vibrational modes for the lowest vibrational states is straightforward and can be done by analysis and visual inspection of the vibrational wavefunctions. However, it becomes more difficult with increasing energy as the modes become mixed and the coordinate system is no longer appropriate[25] for visual assignment of the vibrational modes.

3.2   Rovibrational states and rotational constants

The rovibrational states of the H_2O-HCN cluster for $J = 0, \ldots, 3$ are computed using the quantum mechanical method described above. The convergence of an MCTDH calculation is tested with respect to both bases: the primitive basis and the SPF basis. In this

Table 2 Harmonic and variational intermolecular frequencies of H_2O-HCN. Heikkilä are the results from Heikkilä et al.[14] (MP2 with 6-311++G(2d,2p)), Tshehla are the results from Tshehla and Anthony[68] (MP2 with $6-31G^{**}$ split-valence polarized basis set), Harm are our new CCSD(T)-F12b/VTZ-F12 ab initio harmonic frequencies, and MCTDH corresponds to the results of this work—obtained on the QSD PES at $J = 0$. All energies are in cm^{-1}.

Mode	Heikkilä	Tshehla	Harm	MCTDH
ν_1 (HCN libration)	98.9	57.2	72.7	93.4
ν_2 (H_2O wagging)	101.6	110.0	84.6	110.9
ν_3 (O···C stretch)	139.9	133.8	121.2	130.0
ν_4 (H_2O torsion)	144.6	222.4	147.8	171.6
ν_5 (H_2O rocking)	243.1	255.0	239.1	237.6
ZPE*	364.1	389.2	332.7	357.2

study, we first performed a series of calculations for $J = 0$, varying the SPFs basis sizes to determine the required size to reach convergence. Then, using that SPF basis, we modified the primitive basis to determine an appropriate basis that ensured a converged calculation while balancing computational cost. The primitive basis reported in Table 1 is the one finally selected, and all the results presented in this work were obtained using that basis. Finally, to ensure consistency, we once again vary the SPF basis to ensure that the vibrational levels do not vary significantly. The results of these last convergence tests are presented in Table 3, where we show the convergence of the ground state and the first two excited states with increasing SPFs basis size. As already mentioned, MCTDH calculations are likely to produce real and fictitious states: the states with energy E_1, E_2, E_3, E_4, E_5, and E_6 are two of those states coming directly from MCTDH calculations that we filter out from our results using the analysis procedure described before. By systematically testing the convergence of our results with different basis sizes, we were able to ensure that our calculations are accurate and reliable.

Despite some limitations of the current implementation of the MCTDH method in the Heidelberg MCTDH package (i.e., lack of symmetry of the Wigner-DVR), important information can be obtained from the calculations of Tables 4–7 using various analysis procedures. First, the primitive basis selected for the calculation connects the average value of the angular modes α and ϕ to m_A and m_B respectively, which is necessary to define $K = m_A + m_B$. Thus by simply checking the output file from the MCTDH calculation, the major character ($\Sigma, \Pi, \ldots$) of the eigenstates can be extracted. Tables 4–7 show the energy levels of H_2O-HCN reported relative to the 5D ground state energy at -1457.281 cm^{-1}. In the Tables, the energy levels are labeled with the values of K, the projection of the total angular momentum on the z-axis of the system, with $K = 0$, $K = 1$, $K = 2$, and $K = 3$ corresponding to Σ, Π, Δ, and Φ states respectively.

Second, the 'Weight' and 'Assignment' columns are based on the magnitude of the contribution of each $j_{k_a k_c}$ to the total wavefunction as referenced in the work of Wang and Carrington.[25] A more detailed description of how this procedure has been applied in this context is provided in the Appendix. For this work, we evaluated the weights for the $J = 0, \ldots, 3$ rotational states and

Table 3 Convergence of the ground state rovibrational energy (cm^{-1}) of H_2O-HCN for $J = 0$. In the Table, the first column represents the SPF basis, where $a_1/a_2/a_3$ stands for the number of SPF along the first mode R(After extensive testing along the R mode, we determined that the mode achieves convergence with an SPF value of 8. However, in order to ensure a higher level of accuracy, we have opted to set the SPF value to 10), the second combined mode $Wigner/K/K$, and the third combined mode $KLeg/K$, as suggested in Table 1. The energy E_0 is the ground state energy of this system and E_7 is the first excited state . E_1, E_2, E_3, E_4, E_5, and E_6 are nonphysical energy levels that are filtered out from our results.

SPF	Energy							
	E_0	E_1	E_2	E_3	E_4	E_5	E_6	E_7
10/60/40	**-1457.280**	-1442.897	-1442.897	-1399.824	-1399.824	-1367.465	-1367.464	**-1363.799**
10/70/40	**-1457.280**	-1442.898	-1442.898	-1399.824	-1399.824	-1367.466	-1367.466	**-1363.797**
10/80/40	**-1457.280**	-1442.898	-1442.898	-1399.825	-1399.825	-1367.467	-1367.467	**-1363.803**
10/90/40	**-1457.281**	-1442.898	-1442.898	-1399.825	-1399.825	-1367.467	-1367.467	**-1363.803**
10/100/40	**-1457.281**	-1442.898	-1442.898	-1399.825	-1399.825	-1367.467	-1367.467	**-1363.804**
10/60/50	**-1457.280**	-1442.897	-1442.897	-1399.823	-1399.823	-1367.464	-1367.464	**-1363.799**
10/70/50	**-1457.280**	-1442.898	-1442.898	-1399.825	-1399.825	-1367.466	-1367.465	**-1363.801**
10/80/50	**-1457.280**	-1442.898	-1442.898	-1399.825	-1399.825	-1367.467	-1367.467	**-1363.802**
10/90/50	**-1457.281**	-1442.898	-1442.898	-1399.825	-1399.825	-1367.467	-1367.467	**-1363.803**
10/100/50	**-1457.281**	-1442.898	-1442.898	-1399.825	-1399.825	-1367.467	-1367.467	**-1363.804**
10/60/60	**-1457.280**	-1442.897	-1442.897	-1399.824	-1399.823	-1367.464	-1367.464	**-1363.798**
10/70/60	**-1457.280**	-1442.898	-1442.898	-1399.824	-1399.824	-1367.466	-1367.466	**-1363.802**
10/80/60	**-1457.280**	-1442.898	-1442.898	-1399.824	-1399.824	-1367.467	-1367.467	**-1363.802**
10/90/60	**-1457.281**	-1442.898	-1442.898	-1399.825	-1399.825	-1367.467	-1367.467	**-1363.804**
10/100/60	**-1457.281**	-1442.898	-1442.898	-1399.825	-1399.825	-1367.467	-1367.467	**-1363.804**

neglected the others. As such, the 'Cumulative Weight' that is obtained only sums the contributions of all the partial weights contributions from $J = 0, \ldots, 3$. As the Cumulative Weight is often above 75% and the individual Weight is usually near or above 20%, the rotational state assignment is quite reliable assuming that higher rotational states have a negligible contribution to that specific wavefunction. However, while we attempt to associate a major H_2O rotational character to the rovibrational wavefunctions, it is worth pointing out that for several of these states the contribution of a specific H_2O rotational state was just marginally higher than others, and it is actually more likely that two or three H_2O rotational states contribute to the character of a specific rovibrational state rather than just a single state.

Third, we can also specify the *para/ortho*-H_2O parity of the rovibrational state by assessing the major character obtained in the 'Assignment' column. In fact, the overlaps of the rovibrational wavefunctions are only non-zero for *para/ortho* states according to the character of the most dominant H_2O rotational states. This specific aspect supports the idea that states from different rotational symmetries (*para/ortho*) do not mix in the generation of rovibrational states of the cluster (at least at low energies as displayed here) and thus the implementation of symmetry on the Wigner-DVR in MCTDH, allowing to separate *para* from *ortho* H_2O states in the calculations would definitely help in reducing the cost of the calculations while producing yet accurate results.

One current limitation that we experience however in our setup is the inability to implement the inversion symmetry in the MCTDH code unlike other authors such as Wang and Carrington[25]. The global structure of the MCTDH code requires a particular attention and care in the selection of subroutines that would need to be modified to properly integrate the symmetries. This type of project which is quite significant and is being planned is

also very important as it should enhance the ability of the Heidelberg MCTDH package in dealing with the type of problems and systems that we investigate here.

Table 4 Low energy rovibrational levels of H_2O-HCN for $J = 0$. The definition of weight and cumulative weight (cum. wgt.) is given in the text. p/o-H_2O specifies the *para/ortho*-H_2O character of the rovibrational states. Energies are relative to the ground state at -1457.281 cm^{-1} and are given in cm^{-1}. The weights and cumulative weights are dimensionless.

p/o-H_2O	Assignment	Energy	Weight	Cum. Wgt.
p	$\Sigma(1_{11})$	0.000	0.343	0.934
o	$\Sigma(1_{01})$	93.477	0.224	0.861
o	$\Sigma(1_{01})$	110.989	0.198	0.894
p	$\Sigma(1_{11})$	130.066	0.343	0.913
o	$\Sigma(2_{21})$	171.673	0.328	0.861
p	$\Sigma(1_{11})$	173.234	0.276	0.849
o	$\Sigma(1_{01})$	217.613	0.225	0.856
p	$\Sigma(2_{11})$	224.841	0.253	0.793
p	$\Sigma(2_{11})$	229.862	0.234	0.835
o	$\Sigma(1_{01})$	237.690	0.204	0.898
p	$\Sigma(1_{11})$	253.893	0.341	0.913
o	$\Sigma(2_{12})$	254.397	0.212	0.687
o	$\Sigma(2_{12})$	260.083	0.220	0.755

The calculation and assignment of the rovibrational energy levels allows us to compute the rotational transition frequencies, from which we deduce the rotational constants of the rigid rotor H_2O-HCN system. The rovibrational energy levels of a molecular system can be described by a set of quantum numbers, which represent the rotational and vibrational states of the molecule. In the rigid rotor approximation, H_2O-HCN is an asymmetric ro-

Table 5 Same as Table 4 for $J = 1$.

p/o-H$_2$O	Assignment	Energy	Weight	Cum. Wgt.
p	$\Sigma(1_{11})$	0.205	0.343	0.912
o	$\Sigma(1_{01})$	14.595	0.243	0.899
o	$\Sigma(1_{01})$	14.595	0.243	0.854
p	$\Sigma(1_{11})$	90.031	0.309	0.878
p	$\Sigma(1_{11})$	90.032	0.309	0.878
p	$\Sigma(1_{11})$	93.684	0.309	0.879
o	$\Sigma(1_{01})$	111.194	0.198	0.894
o	$\Sigma(1_{01})$	130.267	0.224	0.856
p	$\Pi(1_{11})$	143.018	0.343	0.913
o	$\Pi(1_{01})$	144.518	0.245	0.900
o	$\Sigma(2_{21})$	171.877	0.328	0.765
p	$\Sigma(1_{11})$	173.442	0.276	0.825
p	$\Pi(1_{11})$	214.898	0.307	0.884
o	$\Sigma(1_{01})$	217.817	0.225	0.856
p	$\Sigma(2_{11})$	225.049	0.253	0.807
p	$\Sigma(2_{11})$	230.101	0.234	0.830
o	$\Sigma(1_{01})$	237.891	0.204	0.898
p	$\Sigma(1_{11})$	254.090	0.341	0.913
o	$\Sigma(2_{12})$	254.601	0.212	0.687
p	$\Pi(1_{11})$	255.658	0.250	0.839
o	$\Sigma(2_{12})$	260.290	0.220	0.752

Table 6 Same as Table 4 for $J = 2$.

p/o-H$_2$O	Assignment	Energy	Weight	Cum. Wgt.
p	$\Sigma(1_{11})$	0.611	0.343	0.912
o	$\Sigma(1_{01})$	15.001	0.243	0.899
o	$\Sigma(1_{01})$	15.003	0.243	0.856
o	$\Delta(1_{10})$	58.101	0.246	0.845
p	$\Sigma(1_{11})$	90.441	0.309	0.883
p	$\Sigma(1_{11})$	90.442	0.309	0.883
o	$\Sigma(1_{01})$	94.095	0.224	0.861
o	$\Sigma(1_{01})$	111.602	0.198	0.888
p	$\Sigma(1_{11})$	130.666	0.343	0.913
o	$\Sigma(1_{01})$	144.919	0.245	0.900
o	$\Sigma(1_{01})$	172.254	0.328	0.861
p	$\Sigma(1_{11})$	173.854	0.276	0.857
p	$\Pi(1_{11})$	215.308	0.307	0.884
o	$\Sigma(1_{01})$	218.223	0.225	0.865
p	$\Sigma(2_{11})$	225.467	0.252	0.803
p	$\Sigma(2_{11})$	230.535	0.234	0.831
p	$\Delta(2_{11})$	236.557	0.244	0.810
o	$\Sigma(1_{01})$	238.292	0.204	0.898
p	$\Sigma(1_{11})$	254.482	0.341	0.913
o	$\Sigma(2_{12})$	255.008	0.212	0.686
p	$\Pi(1_{11})$	256.082	0.251	0.838
o	$\Sigma(2_{12})$	260.701	0.220	0.753

Table 7 Same as Table 4 for $J = 3$.

p/o-H$_2$O	Assignment	Energy	Weight	Cum. Wgt.
p	$\Sigma(1_{11})$	1.215	0.343	0.911
o	$\Sigma(1_{01})$	15.608	0.243	0.899
o	$\Sigma(1_{01})$	15.613	0.243	0.915
p	$\Delta(2_{11})$	58.711	0.285	0.849
p	$\Sigma(1_{11})$	91.055	0.309	0.883
p	$\Sigma(1_{11})$	91.060	0.309	0.883
o	$\Sigma(1_{01})$	94.711	0.224	0.860
o	$\Sigma(1_{01})$	112.215	0.198	0.894
p	$\Sigma(1_{11})$	131.264	0.343	0.913
o	$\Sigma(1_{01})$	145.513	0.245	0.901
p	$\Gamma(1_{01})$	155.500	0.261	0.814
o	$\Sigma(1_{10})$	172.812	0.210	0.860
p	$\Sigma(1_{11})$	174.473	0.276	0.853
p	$\Pi(1_{11})$	215.909	0.307	0.884
o	$\Sigma(1_{01})$	218.882	0.225	0.865
p	$\Sigma(1_{11})$	226.081	0.256	0.805
p	$\Sigma(2_{11})$	231.128	0.234	0.830
p	$\Delta(2_{11})$	237.172	0.245	0.810
o	$\Sigma(1_{01})$	238.959	0.204	0.898
p	$\Sigma(1_{11})$	255.067	0.341	0.913
o	$\Sigma(2_{12})$	255.618	0.212	0.686
p	$\Pi(1_{11})$	256.704	0.251	0.838
o	$\Gamma(3_{12})$	261.059	0.336	0.710
o	$\Sigma(2_{12})$	261.316	0.220	0.753

tor whose rotational states can be described using $j_{K_a K_c}$, where K_a and K_c are specified as above for H$_2$O. Thus, our calculations at $J = 0$ will provide for instance the 0_{00} state (along with various vibrational excitations), while the calculations at $J = 1$ will provide the 1_{01}, 1_{11} and 1_{10} states (with various rovibrational excitations). Although there are currently no experimental rovibra-

tional energy levels available for comparison with the theoretical values, there are some experimental measurements of other spectroscopic properties—such as the rotational constants and transition frequencies—that can be used to assess the accuracy of the theoretical model and provide a mean to validate our results. The theoretical transition frequencies we obtain from our calculations are reported in Table 8 and are in excellent agreement with the observed values by Fillery et al.,[22] the largest error being 0.71%.

In Table 9, calculated rotational constants are determined from the $J = 1, \cdots, 3$ levels. A number of approaches can be used to reasonably estimate the rotational constants of a molecular system from the rovibrational states—such as fitting an expansion with several coefficients. Usually, a first-order approximation which links the rotational energy levels of an asymmetric top for the total angular momentum $J = 1$ ($1_{01} = B + C$, $1_{10} = A + B$ and $1_{11} = A + C$) with $A \neq B \neq C$ is applied. However, in this case this procedure leads to a degeneracy of B and C, because of the near degeneracy of the 2nd and 3rd state obtained in Table 5 at the precision displayed. The values of A, B and C obtained in this case are respectively 434.473 GHz, 3.067 GHz and 3.065 GHz. Here we supplemented these calculations, with the first order approximation of the rotational constants for $J = 2$ and $J = 3$. For $J = 2$ we obtain for A, B and C 434.501 GHz, 3.061 GHz and 3.040 GHz. And for $J = 3$, 434.610 GHz, 3.047 GHz and 3.024 GHz. The values reported in Table 9 is an average for A, B and C of these values.

The comparison of these numerical results with experimentally determined values and also previous calculations shows the qual-

ity of the PES in describing the interactions and provides some confidence in its reliability for collisional dynamics.

Table 8 Selected rotational $j_{K_a K_c}$ transition frequencies of H_2O-HCN, energy units are in cm^{-1}.

Transition	MCTDH	Experiment[22]	% error
$1_{01} \leftarrow 0_{00}$	0.2046	0.2034	0.59
$2_{02} \leftarrow 1_{01}$	0.4079	0.4068	0.27
$2_{11} \leftarrow 1_{10}$	0.4091	0.4075	0.39
$2_{12} \leftarrow 1_{11}$	0.4078	0.4058	0.49
$3_{03} \leftarrow 2_{02}$	0.6138	0.6102	0.59
$3_{12} \leftarrow 2_{11}$	0.6136	0.6113	0.38
$3_{13} \leftarrow 2_{12}$	0.6131	0.6088	0.71

We further investigated the rovibrational energy levels of the H_2O-HCN by examining the wavefunctions associated with each level. These wavefunctions can provide relevant information about the molecular structure and behavior of the heterodimer, the type of motion associated with each vibrational mode, and even the deviation of the progression from the normal mode to local mode behavior. Table 2 summarizes the character of motion associated with the various vibrational modes of H_2O-HCN. Figure 5 describes the mode ν_1, which is the librational motion of the HCN molecule with respect to the H_2O molecule. The libration mode involves the oscillation of the HCN molecule around the γ axis that is perpendicular to the H_2O-HCN bonding axis corresponding to $ortho$-H_2O-HCN Σ state ($K = 0$) $J = 0$ at the equilibrium position where the wavefunction has a maximum located at $R = 7.096$ Bohr. In Figure 6 we also have the $ortho$-H_2O-HCN state assigned to the mode ν_2 which describes the H_2O wagging motion of the water molecule with to the HCN molecule and its plot represents pivoting of the water molecule around its $O-H$ bonding axis of $ortho$-H_2O-HCN Σ state. For $J = 0$, the angular plot at $R = 7.096$ Bohr in Figure 7 shows the mode ν_3 corresponding to the $O \cdots C$ stretch of the wavefunction of $para$-H_2O-HCN state localized near the global minimum with the plot describing the stretching or contracting of the bond between the O-atom of the water molecule and C-atom of the HCN molecule. Figures 8 and 9 show the most excited states localized at the global and secondary minima, with both the same assignment Σ corresponding to H_2O rocking mode corresponding to $para$-H_2O-HCN and $ortho$-H_2O-HCN states respectively.

4   Conclusion

This paper describes the calculation of low-lying rovibrational states of the H_2O-HCN heterodimer in the rigid rotor approximation using the potential energy surface developed by Quintas-Sanchez and Dubernet[15] and the MCTDH method for values of the total angular momentum quantum number J between 0 and 3. The rovibrational states have been reported with considerable detail assigning the $para/ortho$ (p/o) nature of H_2O for each total angular momentum with a computational approach similar to the one previously used by us[26] for the rovibrational states of H_2O-H_2 in the rigid rotor approximation. While the calcula-
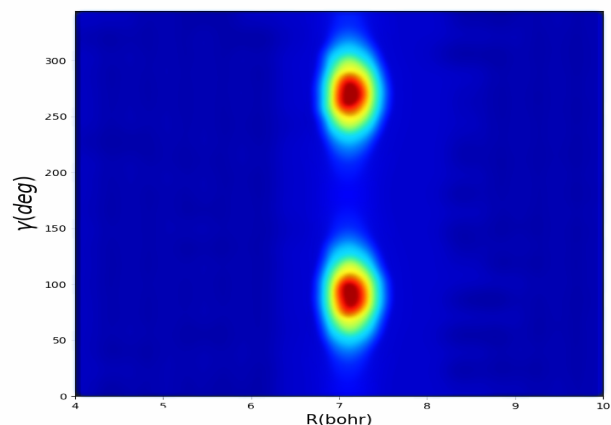

Fig. 5 Wavefunction cut (R, γ) of H_2O-HCN at E= 93.477 cm^{-1}
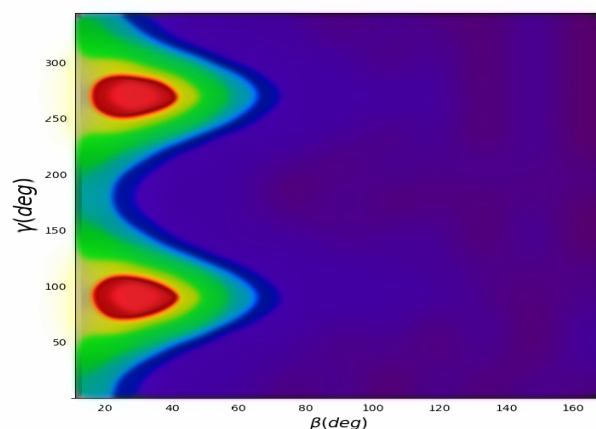
Fig. 6 Wavefunction cut (β, γ) of H_2O-HCN at E= 110.90 cm^{-1}
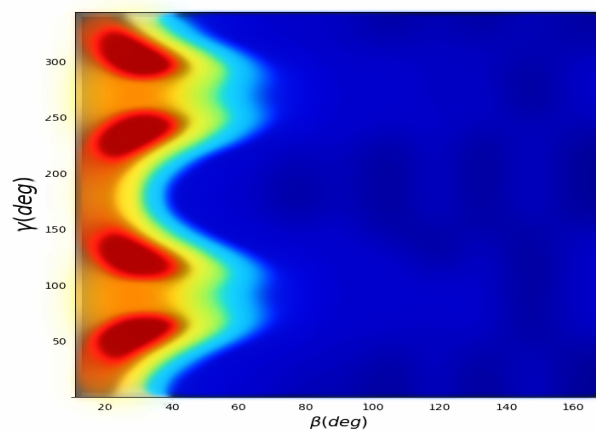
Fig. 7 Wavefunction cut (β, γ) of H_2O-HCN at E= 130.0 cm^{-1}

tion for the specific H_2O-HCN complex is new and we believe deserves to be highlighted here, one of the main ideas of this

Table 9 Calculated rotational constants of H_2O-HCN using MCTDH and compared with the previous theoretical(theo) and experimental(exp) results, units in GHZ. With (Theo1) (CCSD(T)) level of theory[15], (Theo2) MP2/aug-cc-pVTZ level of theory[12], (Theo3) MP2/6-311++G(2df, 2p) level of theory[17], (Theo4) MP2/6-311++G(2df, 2p) level of theory[13], (Theo5) MP2/aug-cc-pVDZ level of theory[19], (Exp1)[22], and (Exp2)[11]

	MCTDH	Theo1	Theo2	Theo3	Theo4	Theo5	Exp1	Exp2
A	434.528	423.753	583.647	402.514	401.031	429.98		
B	3.059	3.073	3.183	3.046	3.046	3.04	3.062	3.046
C	3.043	3.051	3.159	3.026	3.027	3.01	3.037	3.020
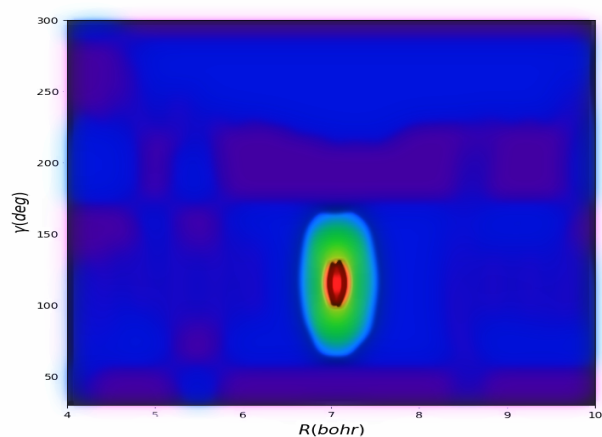
Fig. 8 Wavefunction cut (R, γ) of H_2O-HCN at E= 224.841 cm^{-1}
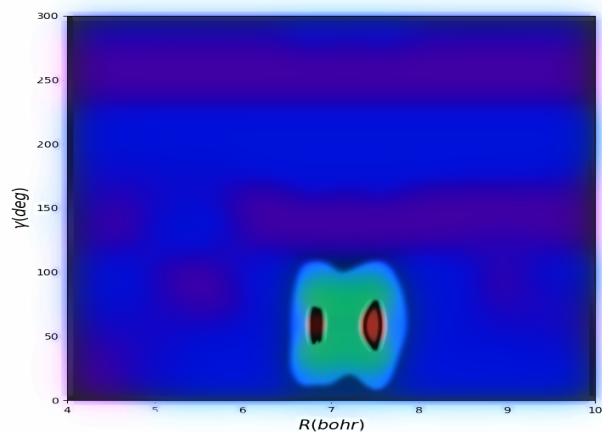
Fig. 9 Wavefunction cut (R, γ) of H_2O-HCN at E= 237.690 cm^{-1}

paper is to present the MCTDH method and code as a reliable tool to perform this type of calculation more routinely: that is spectroscopic calculations involving molecular dimers. Methodologically, we went beyond what was presented in our previous work on H_2O-H_2 by presenting an extensive set of tools that are either already available in the MCTDH code, or that could be implemented with a minimal effort, which could be used to perform a deep analysis of the rovibrational states of a variety of systems and extract their character and symmetry in addition to the transition frequencies, rotational constants, and wavefunctions visualizations. This is particularly useful as there is available an

open source tool (the MCTDH code) that allows the community to study various systems that are relevant to the astrophysics and atmospheric chemistry community. These are presented as alternatives to others such as those by Carrington et al.[69,70] and Bačić et al.[36,71,72]. These last two approach in particular are extremely efficient for this type of applications and this type of systems and others as it has been demonstrated in previous work as they usually allow a significant reduction in the computational resources (time and space) while providing accurate results. However, they both lack one of the major assets we are pushing forward here related to the MCTDH approach and package: those are versatility and open access.

The results presented here show a very good agreement with transition frequencies and rotational constants observed experimentally. However, the lack of experimental rovibrational energies is an opportunity for this system.

In future work, we plan to survey some isotopologues of this system such as the D_2O-HCN which could be relevant for astrophysical applications. Experimental results for isotopically substituted clusters have already been reported. Gutowsky et al.[11] have observed the rotational transition frequencies of the water and hydrogen cyanide dimer using a modified Balle/Flygare Fourier transform microwave spectrometer associated with a sample source pulsed supersonic nozzle. It will be interesting to assess those results in the light of our present calculations. Finally, in the spirit of the work we initiated on H_2O-H_2, we plan to produce converged quantum scattering cross-sections using the MCTDH method which we proved before to be robust enough[49] for this type of study.

Author Contributions

Hervé Tajouo Tela performed the rovibrational calculations, analyzed the results, and contributed to the writing of the manuscript. Ernesto Quintas-Sánchez and Marie-Lise Dubernet computed the PES used for these calculations and contributed to the writing of the manuscript. Yohann Scribano, Fabien Gatti, and Richard Dawes contributed to the analysis of the results and the writing of the manuscript. Steve Ndengué conceptualized and designed the work and contributed to the analysis of the results; he also contributed to the writing of the manuscript.

Conflicts of interest

There is no conflict of interest for this work.

Acknowledgements

The authors would like to acknowledge the support from CINECA for the computational time allocated to ICTP-EAIFR. R.D. and

Appendix

The basis on which each rovibrational state is computed can be written as a sum of the individual basis functions multiplied by some coefficients [25,30],

$$|\Psi\rangle = \sum_{j_A k_A m_A, \mu} C_{j_A k_A m_A, \mu} |j_A, k_A, m_A\rangle |\mu\rangle \qquad (14)$$

Where $\mu = \{j_B(m_B); JKM; n_0\}$ and n_0 labels the radial basis functions. The coefficients discussed in the context of the wave function determine the contribution of each basis function to the overall wave function and depend on the specific rovibrational state of the system.

The rotational wavefunction of an asymmetric top H_2O molecule can be described by $|j_A, k_A, m_A; K_a, K_c\rangle$ with j_A as the total angular momentum, k_A as the projection of the total angular momentum j_A along the principal axis of rotation, m_A, the eigenvalue of j_A onto the laboratory frame(Body-fixed Z-axis) [49]

One can re-expand eqn (14) as

$$|\Psi\rangle = \sum_{j_A K_a K_c m_A, \mu} C_{j_A K_a K_c m_A, \mu} |j_A, m_A, K_a, K_c\rangle |\mu\rangle \qquad (15)$$

The expansion coefficients $C_{j_A K_a K_c m_A, \mu}$ from eqn (15) ,

$$C_{j_A K_a K_c m_A, \mu} = \sum_{k_A} C_{j_A k_A m_A, \mu} \alpha^{(j_A m_A)}_{k_A, K_a K_c} \qquad (16)$$

The coefficients $\alpha^{(j_A m_A)}_{k_A, K_a K_c}$ described in eqn (16) can be obtained by diagonalizing the rotational Hamiltonian of the water monomer in the $|j_A, k_A, m_A\rangle$ basis.

$$|j_A, m_A, K_a, K_c\rangle = \sum_{k_A} \alpha^{j_A m_A}_{k_A, K_a K_c} |j_A, k_A, m_A\rangle \qquad (17)$$

$|j_A, k_A, m_A\rangle$ is the Wigner-D matrix describing the rotation of the molecule from the principal axis frame to the laboratory frame. The contribution of each state $|j_{K_a K_c}\rangle$ form eqn (17 is given by

$$\zeta_{j_A K_a K_c, \mu} = \sum_{\mu} \sum_{m_A} C^2_{j_A K_a K_c m_A, \mu} \qquad (18)$$

We assign the $|j_{K_a K_c}\rangle$ based on the highest magnitude of $\zeta_{j_A K_a K_c, \mu}$. The H_2O nature is para H_2O with $(-1)^{(K_a - K_c)} = +1$ and ortho H_2O with $(-1)^{(K_a - K_c)} = -1$.

Notes and references

1 M. Festou, H. Rickman and R. West, *Astron. Astrophys. Rev.*, 1993, **5**, 37–163.

2 J. Crovisier, N. Biver, D. Bockelée-Morvan and P. Colom, *Plane. Space Sci.*, 2009, **57**, 1162–1174.

3 P. Gerakines, M. Moore and R. Hudson, *Icarus*, 2004, **170**, 202–213.

4 D. A. Smith, *Modeling the hydrogen bond*, ACS Publications, 1994.

5 S. Scheiner *et al.*, *Hydrogen bonding: a theoretical perspective*, Oxford University Press on Demand, 1997.

6 S. J. Grabowski, *Hydrogen bonding: new insights*, Springer, 2006, vol. 3.

7 D. Hadzi, *Theoretical treatments of hydrogen bonding*, John Wiley & Sons Chichester, New York, Weinheim, Brisbane, Singapore, Toronto, 1997.

8 E. Muchová, V. Špirko, P. Hobza and D. Nachtigallová, *Phys. Chem. Chem. Phys.*, 2006, **8**, 4866–4873.

9 Q. Li, X. Wang, J. Cheng, W. Li, B. Gong and J. Sun, *Int. J. Quant. Chem.*, 2009, **109**, 1396–1402.

10 S. Liebman, R. Pesce-Rodriguez and C. Matthews, *Adv. Space Res.*, 1995, **15**, 71–80.

11 H. Gutowsky, T. Germann, J. Augspurger and C. Dykstra, *J. chem. phys.*, 1992, **96**, 5808–5816.

12 T. Malaspina, E. Fileti, J. Riveros and S. Canuto, *J. Phys. Chem. A*, 2006, **110**, 10303–10308.

13 R. Rivelino and S. Canuto, *J. Phys. Chem. A*, 2001, **105**, 11260–11265.

14 A. Heikkilä, M. Pettersson, J. Lundell, L. Khriachtchev and M. Räsänen, *J. Phys. Chem. A*, 1999, **103**, 2945–2951.

15 E. L. Quintas Sanchez and M.-L. Dubernet, *Phys. Chem. Chem. Phys.*, 2017, **19**, 6849–6860.

16 M.-L. Dubernet and E. Quintas-Sánchez, *Molecular Astrophysics*, 2019, **16**, 100046.

17 R. Rivelino and S. Canuto, *Chem. Phys. Lett.*, 2000, **322**, 207–212.

18 L. Turi and J. Dannenberg, *J. Phys. Chem.*, 1993, **97**, 7899–7909.

19 E. E. Fileti, R. Rivelino and S. Canuto, *J. Phys. B: At., Mol. Opt. Phys.*, 2003, **36**, 399.

20 A. Hinchliffe, *J. Mol. Struct.*, 1986, **136**, 193–199.

21 R. Rivelino, *Int. J. Quant. Chem.*, 2011, **111**, 1256–1269.

22 A. Fillery-Travis, A. Legon and L. Willoughby, *Proc. R. Soc. London. Ser. A*, 1984, 405–423.

23 A. J. Fillery-Travis, A. Legon and L. Willoughby, *Chem. Phys. Lett.*, 1983, **98**, 369–372.

24 A. van der Avoird and D. Nesbitt, *J. Chem. Phys.*, 2011, **134**, 044314.

25 X.-G. Wang and T. Carrington Jr., *J. Chem. Phys.*, 2011, **134**, 044313.

26 S. A. Ndengué, Y. Scribano, D. M. Benoit, F. Gatti and R. Dawes, *Chem. Phys. Lett.*, 2019, **715**, 347–353.

27 J. Lundell, *The Journal of Physical Chemistry*, 1995, **99**, 14290–14300.

28 Š. Budzák, P. Carbonniere, M. Medved' and I. Černušák, *Mol. Phys.*, 2014, **112**, 3225–3236.

29 A. Barclay, A. van der Avoird, A. McKellar and N. Moazzen-Ahmadi, *Phys. Chem. Chem. Phys.*, 2019, **21**, 14911–14922.

30 P. M. Felker and Z. Bačić, *J. Chem. Phys.*, 2020, **153**, 074107.

31 P. M. Felker and Z. Bačić, *J. Phys. Chem. A*, 2021, **125**, 980.

32 Y. Liu and J. Li, *Phys. Chem. Chem. Phys.*, 2019, **21**, 24101–24111.

33 Z. Kisiel, A. C. Legon and D. Millen, *Proc. R. Soc. Lond. Ser. A Math. Phys. Sci.*, 1982, **381**, 419–442.

34 J. Loreau, Y. N. Kalugina, A. Faure, A. van Der Avoird and F. Lique, *J. Chem. Phys.*, 2020, **153**, 214301.

35 D. Viglaska, X.-G. Wang, T. Carrington Jr and D. P. Tew, *J. Mol. Spectrosc.*, 2022, **384**, 111587.

36 P. M. Felker and Z. Bačić, *J. Chem. Phys.*, 2022, **156**, 064301.

37 Y. Liu, J. Li, P. M. Felker and Z. Bačić, *Phys. Chem. Chem. Phys.*, 2021, **23**, 7101–7114.

38 P. M. Felker and Z. Bačić, *Chin. J. Chem. Phys.*, 2021, **34**, 728–740.

39 M. Masia, H. Forbert and D. Marx, *J. Phys. Chem. A*, 2007, **111**, 12181–12191.

40 H.-D. Meyer, U. Manthe and L. S. Cederbaum, *Chem. Phys. Lett.*, 1990, **165**, 73–78.

41 U. Manthe, H.-D. Meyer and L. S. Cederbaum, *J. Chem. Phys.*, 1992, **97**, 3199–3213.

42 *Multidimensional Quantum Dynamics: MCTDH Theory and Applications*, ed. H. D. Meyer, F. Gatti and G. A. Worth, Wiley-VCH: Weinheim, 2009.

43 M. H. Beck, A. Jäckle, G. A. Worth and H. D. Meyer, *Phys. Rep.*, 2000, **324**, 1–105.

44 Z. Bačić and J. C. Light, *J. Chem. Phys.*, 1986, **85**, 4594.

45 Z. Bačić and J. C. Light, *J. Chem. Phys.*, 1987, **86**, 3065.

46 J. C. Light and T. Carrington Jr., *Adv. Chem. Phys.*, 2000, **114**, 263–310.

47 F. Gatti and C. Iung, *Phys. Rep.*, 2009, **484**, 1–69.

48 S. Ndengué, R. Dawes, F. Gatti and H. D. Meyer, *Chem. Phys. Lett.*, 2017, **668**, 42.

49 S. Ndengué, Y. Scribano, F. Gatti and R. Dawes, *J. Chem. Phys.*, 2019, **151**, 134301.

50 G. Brocks, A. V. D. Avoird, B. T. Sutcliffe and J. Tennyson, *Mol. Phys.*, 1983, **50**, 1025.

51 S. A. Ndengue, R. Dawes and F. Gatti, *J. Phys. Chem. A*, 2015, **119**, 7712.

52 C. Leforestier, *J. Chem. Phys.*, 1994, **101**, 7357–7363.

53 D. Hou, Y.-T. Ma, X.-L. Zhang and H. Li, *J. Chem. Phys.*, 2016, **144**, 014301.

54 F. C. DeLucia, P. Helminger and W. H. Kirchhoff, *J. Phys. Chem. Ref. Data*, 1974, **3**, 211–219.

55 A. G. Maki, W. B. Olson and R. L. Sams, *J. Mol. Spec.*, 1970, **36**, 433–447.

56 O. Denis-Alpizar, T. Stoecklin, P. Halvick and M.-L. Dubernet, *J. Chem. Phys.*, 2013, **139**, 034304.

57 A. Jäckle and H. D. Meyer, *J. Chem. Phys.*, 1996, **104**, 7974–7984.

58 A. Jäckle and H. D. Meyer, *J. Chem. Phys.*, 1998, **109**, 3772–3779.

59 G. Worth, M. Beck, A. Jäckle and H. D. Meyer, *The MCTDH Package, Version 8.2, (2000), University of Heidelberg, Heidelberg, Germany. H.-D. Meyer, Version 8.3 (2002), Version 8.4 (2007), O. Vendrell and H.-D. Meyer, Version 8.5 (2011)*, 2007, See http://mctdh.uni-hd.de.

60 M. Schröder and H.-D. Meyer, *J. Chem. Phys.*, 2017, **147**, 064105.

61 F. Otto, *J. Chem. Phys.*, 2014, **140**, 014106.

62 M. Schröder, *J. Chem. Phys.*, 2020, **152**, 024108.

63 L. J. Doriol, F. Gatti, C. Iung and H.-D. Meyer, *J. Chem. Phys.*, 2008, **129**, 224109.

64 H. D. Meyer and G. A. Worth, *Theor. Chem. Acc.*, 2003, **109**, 251–267.

65 H. D. Meyer, F. L. Quéré, C. Léonard and F. Gatti, *Chem. Phys.*, 2006, **329**, 179–192.

66 R. Kosloff and H. Tal-Ezer, *Chem. Phys. Lett.*, 1986, **127**, 223–230.

67 E. Davidson, *J. Comp. Phys.*, 1975, **17**, 87.

68 T. A. Tshehla, Tankiso M.* & Ford, *S. Afr. J. Chem.*, 1995, **48**, 127–134.

69 X. Wang and T. Carrington Jr., *J. Chem. Phys.*, 2008, **129**, 234102.

70 X. Wang and T. Carrington Jr., *J. Chem. Phys.*, 2023, **158**, 084107.

71 P. M. Felker and Z. Bačić, *J. Chem. Phys.*, 2022, **157**, 194103.

72 P. M. Felker and Z. Bačić, *J. Chem. Phys.*, 2023, **158**, 234109.